Macroscopic, Flexible, High-Performance Graphene Ribbons

Jiankun Sun,[†,‡] Yanhui Li,[†,*] Qingyu Peng,[§] Shaocong Hou,[⊥] Dechun Zou,[⊥] Yuanyuan Shang,[§] Yibin Li,[§] Peixu Li,[∥] Qiuju Du,[†] Zonghua Wang,[†] Yanzhi Xia,[†] Linhua Xia,[†] Xianglong Li,[¶] and Anyuan Cao[‡,*]

[†]Laboratory of Fiber Materials and Modern Textile, the Growing Base for State Key Laboratory, Qingdao University, 308 Ningxia Road, Qingdao 266071, People's Republic of China, [‡]Department of Materials Science and Engineering, College of Engineering, Peking University, Beijing 100871, People's Republic of China, [§]Centre for Composite Materials and Structures, Harbin Institute of Technology, Harbin 150080, People's Republic of China, [⊥]College of Chemistry and Molecular Engineering, Peking University, Beijing 100871, People's Republic of China, [∥]Department of Mechanical Engineering, Tsinghua University, Beijing 100084, People's Republic of China, and [¶]National Center for Nanoscience and Technology, Beijing 100190, People's Republic of China

ABSTRACT Tailoring the structure and properties of graphene fibers is an important step toward practical applications. Here, we report macroscopic, long graphene ribbons formed by combining electrostatic interaction and shear stress during the wet-spinning process. The graphene ribbons are flexible and can be woven into complex structures, and the ribbon morphology can be tailored by controlling the orientation of wrinkles to obtain elasticity within a modest strain. We demonstrate several potential applications of pure or Pt–graphene hybrid ribbons as elastic strain sensors, counter electrodes for dye-sensitized fiber solar cells with cell efficiencies reaching 4.69% under standard illumination and 6.41% with a back reflector, and woven fabric supercapacitor electrodes. Our method can directly fabricate meter-long graphene ribbons with controlled structure and high performance as both energy conversion and energy storage materials.

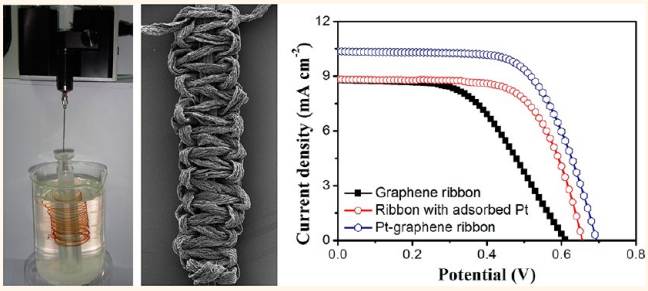

KEYWORDS: graphene ribbon · strain sensor · fiber solar cell · supercapacitor · electrode

Recently, there is a growing research interest in graphene fibers, a macroscopic architecture built from two-dimensional nanoscale graphene oxide (GO) sheets.[1−5] Similar to three-dimensional highly porous graphene aerogels,[6−9] fabrication of graphene fibers with controlled structure and properties opens a possible way to translate the outstanding mechanical and electronic properties of individual graphene sheets into well-defined macrostructures through large-scale self-assembly, thus facilitating practical applications. To this end, a variety of assembly and spinning techniques have been developed to produce continuous fibers with good flexibility, strength, and electrical conductivity.[1−5,10−12] Wet-spinning techniques based on liquid-crystalline or dispersed GO solutions and different coagulation baths have been widely studied.[2−5] Qu *et al.* sealed a GO suspension into a glass pipeline to confine the hydrothermal treatment and form reduced fibers.[1] Also, a chemical vapor deposition (CVD) graphene film floating on a liquid surface can be drawn into a fiber.[12] Alternatively, an aligned multiwalled carbon nanotube sheet can be converted into a graphene nanoribbon yarn by chemical unzipping.[13]

In addition, there are some efforts in controlling the structure and properties of graphene fibers and exploring potential applications. Qu *et al.* fabricated graphene microtubings with site-specific functionalization and hollow fibers with a necklace structure.[14,15] Freeze-drying a graphene fiber by liquid nitrogen during wet-spinning resulted in the formation of a highly porous structure.[16] Coagulation baths containing different surfactants, cationic ions, and polymers have been used to spin graphene fibers with improved mechanical properties.[3−5] Ag nanowires have been incorporated into graphene fibers to improve the electrical conductivity and make stretchable conductors.[10] Based on these fiber structures, a number of applications have been demonstrated such as photosensors,

* Address correspondence to liyanhui@tsinghua.org.cn, anyuan@pku.edu.cn.

Received for review August 30, 2013 and accepted October 28, 2013.

Published online October 28, 2013
10.1021/nn404533r

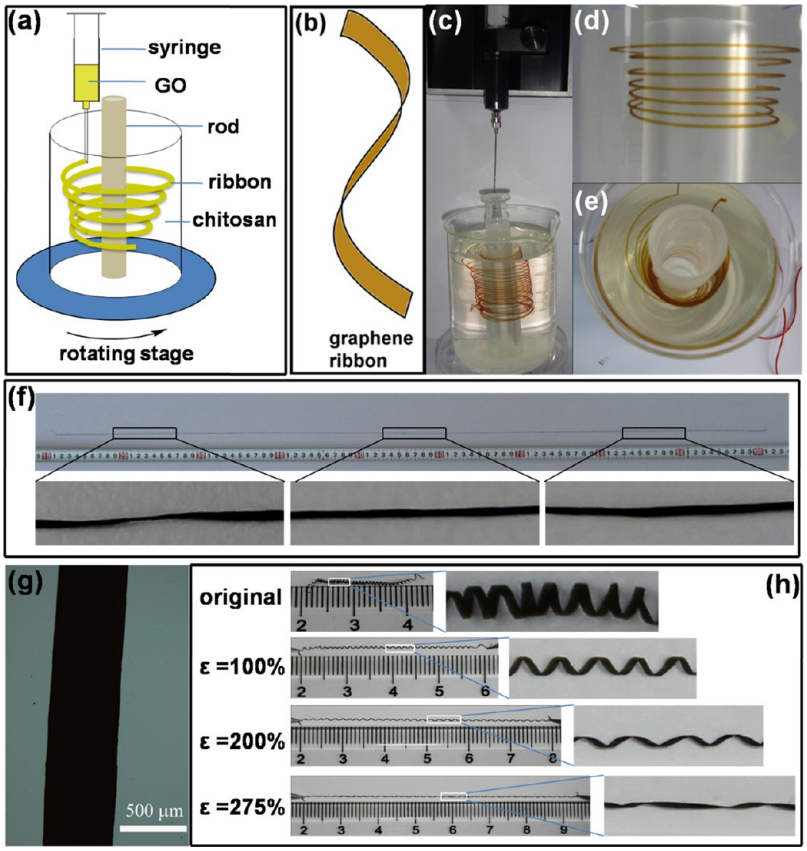

Figure 1. Fabrication of continuous graphene ribbons. (a) Illustration of the wet-spinning setup. (b) Illustration of a flexible ribbon structure. (c) Photo of the setup with a uniform GO ribbon spun in the chitosan solution. (d) Photo of a single ribbon rotating around the collecting rod. (e) Top view of the setup. (f) Photo of a 1 m long, 300 μm wide graphene ribbon after chemical reduction. (g) Opitcal image of a 500 μm wide ribbon. (h) Ribbon made into sprial shape which can be stretched to large strains.

electromechanical systems, flexible electrodes, and field emitters.[10−14] However, the above research remains at the beginning stage, and there are a lot of opportunities in further controlling the fiber structure, tailoring properties, and exploring new applications.

Previously, carbon nanotubes have been successfully spun into various macroscopic structures such as yarns, ribbons, or sheets with many applications.[17−21] However, the morphology of reported graphene fibers is rather limited; for example, ribbons have not been achieved by assembling graphene sheets. Here, we show that, by a modified wet-spinning method, macroscopic graphene ribbons could be fabricated controllably. We introduced shear stress during wet-spinning to produce flat, uniform ribbons with high flexibility. Our graphene ribbons demonstrated high performance in many applications such as elastic strain sensors, flexible counter electrodes for fiber solar cells, and fabric electrodes for supercapacitors.

RESULTS AND DISCUSSION

Our wet-spinning setup is illustrated in Figure 1a. GO sheets were prepared by a modified Hummer's method and had average sizes of several micrometers and few-layer sheets (Supporting Information, Figure S1). A GO suspension in water with a concentration of 6 mg/mL was injected by a syringe pump into a chitosan solution placed on a stage rotating constantly at a speed of 10 rpm. A glass rod was placed vertically in the chitosan solution to collect the GO ribbon and serve as a substrate for subsequent reduction and morphology control. During spinning, the fluid flow direction was perpendicular to the direction along which the GO suspension was injected (downward). We found that the shear stress applied by the viscous chitosan could produce continuous ribbons following the fluid flow and rotating around the rod in the center. Compared to previous graphene fibers, our ribbons exhibited unique structure features including a flat morphology with a large width-to-thickness ratio (up to 100) (Figure 1b). A similar setup was used for spinning carbon nanotube ribbons and fibers in polyvinyl alcohol solution.[21] Here, we adopted the glass rod to facilitate an ordered assembly of GO ribbons during spinning in a viscous solution (Figure 1c−e). The formation of the ribbon structure was mainly due to two factors including the electrostatic interaction between GO sheets and chitosan (as coagulation bath) and the larger shear fluid flow velocity compared to the injection rate of GO suspension. Typically, the ribbon width

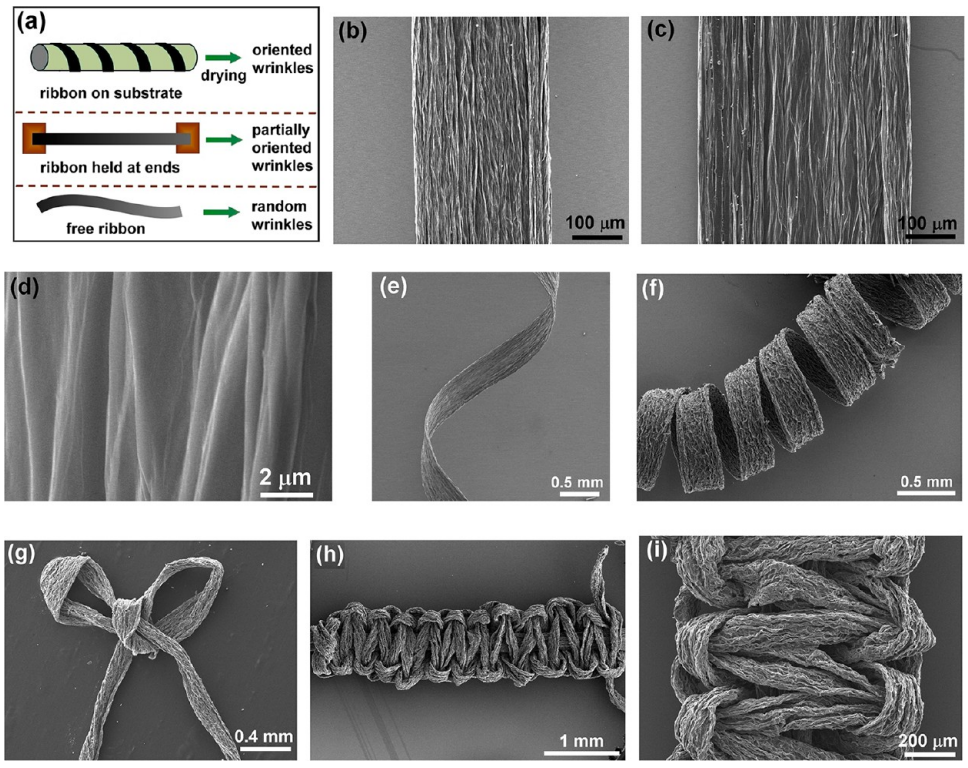

Figure 2. Structural characterization on graphene ribbons. (a) Illustration of different drying conditions that produce ribbons with oriented, partially oriented, or random wrinkles. (b) SEM image of a 262 μm wide ribbon with oriented wrinkles. (c) SEM image of 415 μm wide ribbon. (d) Close view showing a clean ribbon surface with wrinkles. (e) Flexible ribbon. (f) Spring-like loops made by a ribbon. (g) Graphene butterfly knot. (h) Graphene flat knot. (i) Close view showing highly twisted, complex structure in the flat knot.

(200−500 μm) was determined by the diameter of the syringe outlet (a tilted opening in a needle). We have identified a few factors related to the spinning process that may be optimized to tailor the morphology and property of ribbons, including the GO and chitosan concentration, injection rate of GO and rotation speed of chitosan, and the width of the syringe outlet (Figure S2). For example, an optimal concentration range of 5−9 mg/mL was used to ensure continuous spinning with sufficient electrostatic interaction.

By this way, we could reliably produce meter-long, reduced GO ribbons with uniform width (Figure 1f,g). Chemical reduction by hydroiodic acid was carried out on as-spun GO ribbons, which changed the product color from brown to black and made the ribbon conductive (conductivities of 100−150 S/cm). In particular, the use of hydroiodic acid could dissolve the chitosan attached to the ribbon surface, resulting in a clean and pure ribbon without other surfactants, cross-linking ions, or polymers. X-ray diffraction (XRD) measurements showed that the interlayer distance of GO sheets was decreased from 8.600 Å (2θ = 10.3°) in original ribbons to 3.713 Å (2θ = 24.0°) in reduced ribbons due to elimination of oxygen-containing groups on the GO sheets (Figure S1).

The graphene ribbons could be manipulated macroscopically; for example, a wet ribbon was wound around a thin glass capillary to form a stable helical shape after drying (Figure 1h). This spring-like structure was then manually stretched from initially 2 cm to a final length of 7.5 cm, corresponding to a tensile strain of 275%. Although the helical loops have been almost straightened at this large strain, the twisted ribbon did not fracture and could recover to close to original shape, indicating good flexibility and strength.

We have applied different loading conditions on the wet graphene ribbons (after chemical reduction and during the drying process) to control the orientation of wrinkles and the ribbon morphology (Figure 2a). A detail analysis has revealed that the surface tension forces produced during drying are the main factor that causes buckling instability and wrinkles in the GO phases.[22] In our first method, ribbons with different widths were wound around glass rods to make close contact, resulting in strong interaction with the substrate that can counteract the surface tension force and form oriented wrinkles along the length direction, as characterized by scanning electron microscopy (SEM) (Figure 2b−d). Second, a freestanding ribbon was held by its ends vertically or horizontally, resulting in partially oriented wrinkles containing two main orientations along the length (body part) and radial (surface layer) directions (Figure S3). Last, a ribbon was placed in a free state in which extensive random wrinkles

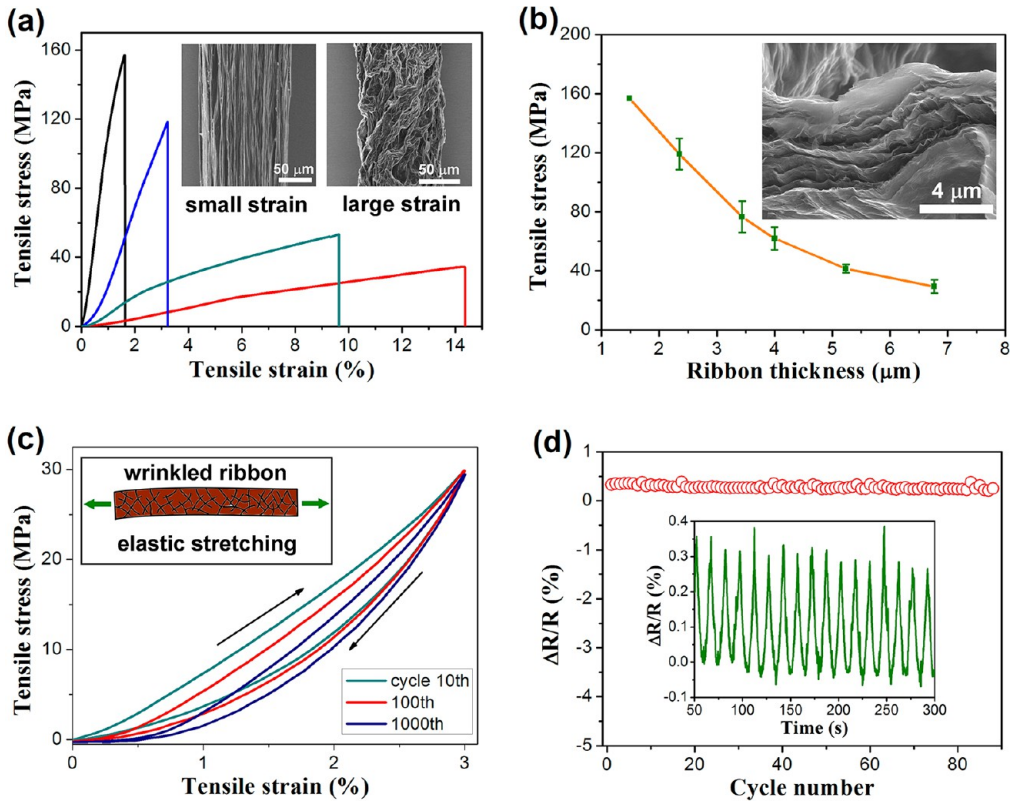

Figure 3. Mechanical properties of graphene ribbons. (a) Tensile stress−strain curves of graphene ribbons with different wrinkle structures. Insets show typical ribbon morphologies producing small (<4%) or relatively large (>9%) tensile strains. (b) Tensile stresses measured in ribbons with different thicknesses. Inset shows the cross section of a fractured ribbon. (c) Cyclic tension test on a wrinkled ribbon within a strain of 3% (selected cycle 10th, 100th, and 1000th are plotted). Inset shows elastic stretching of a ribbon. (d) Relative resistance change ($\Delta R/R$) recorded for 90 stretching cycles. Inset shows the evolution of $\Delta R/R$ over time during cyclic test.

without a particular orientation formed after drying (Figure S3). In comparison, ribbons dried on the substrate showed the most consistent orientation of wrinkles and a relatively smooth surface, while a freely drying ribbon was highly wrinkled with a rough morphology.

Compared to previous graphene fibers, our flexible ribbons were more suitable to form microscale helical structures and woven into various configurations. The graphene ribbons could form stable, spring-like loops with different pitches and simple butterfly knots (Figure 2e−g). Furthermore, a flat knot was made by tying and twisting one ribbon onto a support (straight) ribbon repeatedly and tightly, showing the ability of the graphene ribbon to sustain a lot of twists and assemble very complex, periodic configurations (Figure 2h,i). Tailored morphology and various woven structures shown in the graphene ribbons are useful for further exploring applications.

The orientation of wrinkles directly influenced mechanical properties of graphene ribbons. Uniaxial tension tests revealed two typical fracture behaviors characterized by relatively small ($\varepsilon < 4\%$) or large ($\varepsilon > 9\%$) failure strains in ribbons with oriented or random wrinkles, respectively (Figure 3a). For the former, the tensile stress present during the drying process resulted in improved alignment of graphene sheets and denser stacking between graphene layers, leading to higher strengths (>100 MPa). For the latter, its highly wrinkled structure could sustain a moderate tensile strain (up to about 14%) before fracture, but with a lower strength due to larger intersheet distance. In comparison, most of the previous graphene fibers showed relatively small fracture strains ($\varepsilon < 4\%$), although a few reports obtained higher strains ($\varepsilon < 10\%$) in fibers consisting of GO sheets cross-linked by cationic ions.[2−4] We also varied the chitosan fluid velocity (10−20 rpm) during spinning to produce ribbons with different thicknesses, in which increasing fluid velocity reduced ribbon thickness for the same GO concentration and injection rate. Statistic data showed that the tensile strengths of graphene ribbons increased consistently with reduced thickness from about 7 to 1.5 μm (Figure 3b). Thicker ribbons had more internal empty space, which could weaken the interaction between graphene sheets and lower the ribbon strength. We used SEM to characterize the fractured cross section of the ribbons and measure their average thicknesses, which typically showed a layered structure (inset in Figure 3b).

Those highly wrinkled ribbons were elastic within a modest strain range ($\varepsilon < 5\%$). To study this, a ribbon

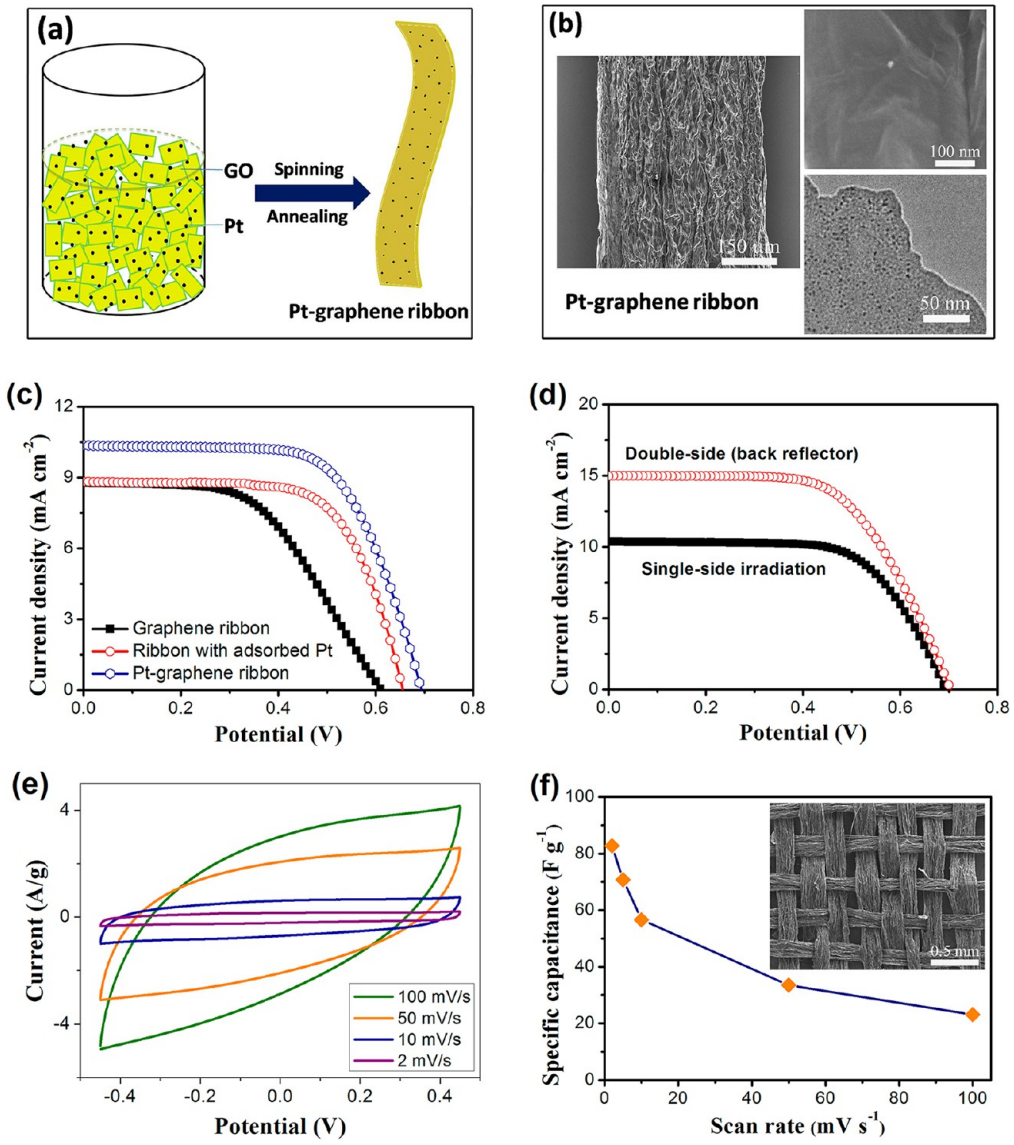

Figure 4. Applications as fiber solar cell and supercapacitor electrodes. (a) Illustration of the process from a Pt-dispersed GO suspension to a Pt−graphene hybrid ribbon by spinning and annealing. (b) SEM images (low and high magnification) of the Pt−graphene ribbon and TEM image of the Pt-grafted GO sheets. (c) *J*−*V* curves of fiber solar cells with counter electrodes of a graphene ribbon, a ribbon with adsorbed Pt nanoparticles on the surface, and a Pt−graphene hybrid ribbon, respectively. (d) *J*−*V* curves of a fiber cell with a Pt−graphene ribbon electrode working in single-side and double-side (with a back reflector) irradiation conditions. (e) CV curves of a supercapacitor using a graphene ribbon fabric as electrode. (f) Specific capacitances calculated at different scan rates. Inset shows the SEM image of the fabric.

was stretched by the two ends to a predefined strain (ε = 3%) for 1000 loading and unloading cycles, and the corresponding stress−strain (σ−ε) curves were recorded (Figure 3c). Elastic stretching was stabilized after several cycles with a linear loading stage and a modulus of about 1 GPa, and the maximum stress was maintained during the following cycles. After 1000 cycles, the ribbon showed negligible permanent deformation as seen from the unloading curve. Such elasticity was attributed to the presence of random wrinkles in the ribbon with similar morphology to the samples producing large strain in Figure 3a, which could be deformed to a certain degree reversibly. Elastic graphene fibers have not been reported so far. In addition, we monitored the electrical resistance (R) simultaneously during cyclic tests and observed reproducible relative resistance change ($\Delta R/R$) for many cycles (stretching to ε = 3% repeatedly), indicating a stable ribbon structure (Figure 3d). Currently, although the resistance changed instantaneously with applied strain, the value of $\Delta R/R$ remained relatively small (about 0.4%), which might be further improved by controlling the wrinkled structure of ribbons. This result indicated potential applications as flexible fiber or ribbon-based strain sensors.

We further applied the graphene ribbons as electrodes for fiber solar cells and supercapacitors. The dye-sensitized fiber solar cell was made by a TiO_2 porous

film coated on a Ti wire as primary electrode and a graphene ribbon (as counter electrode) placed in parallel and contact to the TiO_2 film. The cell with electrolyte was encapsulated in a glass tube. We first dispersed Pt nanoparticles (diameters 2−3 nm) into the GO solution and made a Pt−graphene hybrid ribbon by spinning and thermal annealing to improve the Pt adhesion on graphene (Figure 4a). SEM characterization on the hybrid ribbon (with <1 wt % Pt loading) showed no big aggregations on the ribbon surface, while the TEM image revealed fine particles uniformly grafted on the graphene sheets (Figure 4b). Therefore, well-dispersed and uniformly distributed Pt particles were introduced into the ribbon. A control sample was also made by immersing a graphene ribbon into Pt colloid to adsorb Pt particles on the surface only, which showed larger size clusters due to particle aggregation (Figure S4). The current density−voltage (J−V) characteristics of fiber solar cells with different electrodes (working length = 5 mm) were recorded under air mass of 1.5 and 100 mW cm^{-2} light intensity (Figure 4c). The graphene ribbon exhibited a short-circuit current density (J_{sc}) of 8.77 mW cm^{-2}, an open-circuit voltage (V_{oc}) of 0.61 V, and a power conversion efficiency of 2.80%. The ribbon with adsorbed Pt clusters by immersing showed an increased efficiency of 3.87%. In comparison, the Pt−graphene ribbon produced a J_{sc} of 10.36 mW cm^{-2}, a V_{oc} of 0.69 V, and an efficiency of 4.69%. The highest efficiency was achieved in the hybrid ribbon with uniform Pt particles, owing to a simultaneous enhancement of J_{sc} and V_{oc}. In particular, the fill factor (FF) reached 65%, indicating that a high-performance fiber solar cell has been fabricated. Previous work has demonstrated enhanced catalytic activity by attaching Pt particles to graphene sheets.[23] Our team also reported fiber cells with Pt-adsorbed carbon nanotube yarns as counter electrodes.[24] A TiO_2 nanotube-based fiber cell with higher efficiency was reported by electrodeposition of Pt particles onto graphene fibers, yet with a much higher Pt loading (up to 20 wt %).[25] The cell efficiency can be further improved to 6.41% under double-side irradiation using a diffusive reflector to reflect incident light to the back side of the fiber (Figure 4d). For longer fiber cells, we observed performance degradation with increasing length (from 5 to 50 mm) due to increased resistance of graphene ribbons (Figure S5).

To make a supercapacitor electrode, about 20 graphene ribbons were woven into a freestanding fabric and tested in a three-electrode setup in aqueous electrolyte. Cyclic voltametry (CV) curves showed a nearly rectangular and symmetric shape at lower scan rates, indicating a typical capacitor behavior (Figure 4e). The specific capacitance based on this single-layer ribbon fabric with thickness of <20 μm reached 82.8 F g^{-1} at 2 mV s^{-1} and decreased at increasing scan rates (Figure 4f). The first Coulombic efficiency calculated from the charge−discharge curve is about 93%. Supercapacitors based on graphene aerogels or networks have been extensively studied, and recently, graphene fibers also have been constructed into fiber and textile devices.[7,26,27] Here, our flat ribbons are very suitable to fabricate large-area, thin, flexible devices. The supercapacitor performance might be further improved by creating three-dimensional fabric structure and grafting pseudomaterials.

CONCLUSION

A graphene-based macroscopic structure, graphene (and hybrid) ribbon, was synthesized by a scalable wet-spinning technique. The ribbons showed excellent mechanical properties and potential applications as electrodes in solar cells and supercapacitors. In particular, a Pt−graphene hybrid ribbon with very low Pt loading (<1 wt %) could significantly improve the fiber solar cell performance. Flexible graphene ribbons with tailored morphology have potential applications in many areas such as sensors, actuators, and electrodes.

EXPERIMENTAL SECTION

Preparation of Graphene Ribbons and Pt-Adsorbed Ribbons. GO sheets (with single- to few-layer) were prepared by expanded graphite according to the modified Hummers' method. A homogeneous GO suspension (6 mg/mL) was injected (by a syringe pump at an injection rate of 0.5 mL/min) into a coagulation bath made of 3 g of chitosan, 10 mL of acetic acid, and 500 mL of H_2O. The chitosan bath was placed on a stage constantly rotating at 10−20 rpm during wet-spinning. At the end of spinning, the rotational speed was increased to make the GO ribbons attach closely to the collecting rod. The collecting rod was transferred to an aqueous solution of hydroiodic acid (50%) and soaked for 3 h to dissolve chitosan on the surface of GO ribbons and then kept at 353 K for 2 h for chemical reduction into graphene ribbons. To fabricate Pt−graphene ribbons, 15 mL of GO suspension (6 mg/mL) was first mixed with 100 μL of Pt nanoparticle colloid (20 mM) and then stirred for 5 h to let Pt nanoparticles adsorb onto the GO sheets. Pt colloid with particle sizes of 2−3 nm was synthesized by a solution process using H_2PtCl_6 as precursor. The mixed suspension was then spun into Pt−GO ribbons and reduced to Pt−graphene ribbons by HI. Alternatively, a reduced ribbon was immersed into the Pt colloid to adsorb Pt particles on the surface.

Fabrication of Fiber Solar Cells with Graphene Ribbon Counter Electrode. The photoanode of fiber solar cells was made by dip-coating a TiO_2 colloid onto a Ti wire (diameter 250 μm) and thermal annealing at 300 °C for 5 min. This process was repeated several times to obtain a porous TiO_2 film with a thickness of 10−15 μm. The TiO_2-based primary electrode was sensitized with dye N719. Subsequently, a graphene ribbon or Pt−graphene ribbon was attached to one side of the TiO_2 electrode and then inserted into a glass capillary (inner and outer diameters of 0.9 and 1.2 mm) filled with liquid acetonitrile electrolyte containing 0.03 M iodine, 0.5 M 1-butyl-3-methylimidazolium iodide, 0.3 M *tert*-butyl pyridine, 0.05 M lithium perchlorate, and 0.05 M guanidine thiocyanate. Thermal annealing at 600 °C in Ar/H_2 was performed on the graphene or hybrid ribbons before device assembly. The graphene ribbon was

connected to a Ag wire as counter electrode. Then the ends of the glass capillary were sealed with paraffin wax. Fiber solar cells with working electrode lengths of 5−50 mm were fabricated and tested. During simulated solar irradiation, the graphene ribbon side was placed behind to avoid block of incident light. For double-sided irradiation, a diffuse reflector was placed underneath to reflect light onto the back side of the fiber cell. The current−voltage curves of solar cells were collected in a solar simulator (Yamashit DESO, Japan) at a light intensity of 100 mW cm^{-2} (calibrated by standard silicon solar cell).

Structural Characterization and Measurements. The morphology and structure of GO sheets and graphene ribbons were characterized by SEM (Hitachi S4800) and TEM (FEI Tecnai G2 T20). Raman spectra were recorded on a confocal laser micro-Raman spectrometer (Renishaw in Via plus). XRD was performed in a Bruker D8 diffractometer with Cu Kα radiation (λ = 1.54 Å) for a 2θ range of 5 to 40°. Atomic force microscope (AFM) images on GO sheets were recorded in SPM 5100 (Agilent Technologies).

Mechanical measurements were conducted on a single-column testing instrument (Instron 5843) equipped with a load cell of 10 N. The two ends of a graphene ribbon were fixed on a paper sheet with a cut window by polyvinyl alcohol as adhesive paint. The paper was clamped by grips designed for small-size fiber samples. For stress−strain test, the displacement speed was set as 0.5 mm/min. For cyclic test, the ribbon was stretched to a maximum strain of 3% for 1000 cycles, and the electrical resistance of the graphene ribbon was recorded simultaneously by a Keithley 2400.

Electrochemical measurements (supercapacitor performance) were carried out in a CHI 660D electrochemical station using a three-electrode setup. A fabric of woven graphene ribbons was used as freestanding electrode, with a platinum wire and a saturated calomel electrode (SCE) as counter and reference electrodes, respectively. CV measurements were carried out in a 2 M KCl aqueous electrolyte at room temperature, under an applied potential window ranging from −0.45 to 0.45 V.

Conflict of Interest: The authors declare no competing financial interest.

Acknowledgment. The authors thank Dr. S. Zhang and D. Liu for helpful discussions on fiber solar cell tests. A.C. acknowledges the Natural Science Foundation in China (NSFC program number 91127004) and the research found for the doctoral program of higher education (MOE 08600-452-10132-007). Y.L. acknowledges the Natural Science Foundation of Qingdao (12-1-4-2-23-jch) and National Key Basic Research Development Program of China (973, 2012CB722705).

Supporting Information Available: More SEM characterization on graphene oxide sheets, graphene ribbons, Pt−graphene hybrid ribbons, and data on fiber solar cells. This material is available free of charge *via* the Internet at http://pubs.acs.org.

REFERENCES AND NOTES

1. Dong, Z. L.; Jiang, C. C.; Cheng, H. H.; Zhao, Y.; Shi, G. Q.; Lan, J.; Qu, L. T. Facile Fabrication of Light, Flexible and Multifunctional Graphene Fibers. *Adv. Mater.* **2012**, *24*, 1856–1861.
2. Xu, Z.; Gao, C. Graphene Chiral Liquid Crystals and Macroscopic Assembled Fibres. *Nat. Commun.* **2011**, *2*, 571–579.
3. Cong, H. P.; Ren, X. C.; Wang, P.; Yu, S. H. Wet-Spinning Assembly of Continuous, Neat, and Macroscopic Graphene Fibers. *Sci. Rep.* **2012**, *2*, 613–619.
4. Xu, Z.; Sun, H. Y.; Zhao, X. L.; Gao, C. Ultrastrong Fibers Assembled from Giant Graphene Oxide Sheets. *Adv. Mater.* **2013**, *25*, 188–193.
5. Jalili, R.; Aboutalebi, S. H.; Esrafilzadeh, D.; Shepherd, R. L.; Chen, J.; Aminorroaya-Yamini, S.; Konstantinov, K.; Minett, A. I.; Razal, J. M.; Wallace, G. G. Scalable One-Step Wet-Spinning of Graphene Fibers and Yarns from Liquid Crystalline Dispersions of Graphene Oxide: Towards Multifunctional Textiles. *Adv. Funct. Mater.* **2013**, 10.1002/adfm.201300765.
6. Wang, J.; Ellsworth, M. Graphene Aerogels. *ECS Trans.* **2009**, *19*, 241–247.
7. Zhang, X. T.; Sui, Z. Y.; Xu, B.; Yue, S. F.; Luo, Y. J.; Zhan, W. C.; Liu, B. Mechanically Strong and Highly Cnductive Graphene Aerogel and Its Use as Electrodes for Electrochemical Power Sources. *J. Mater. Chem.* **2011**, *21*, 6494–6497.
8. Xu, Y. X.; Sheng, K. X.; Li, C.; Shi, G. Q. Self-Assembled Graphene Hydrogel *via* a One-Step Hydrothermal Process. *ACS Nano* **2010**, *4*, 4324–4330.
9. Hu, H.; Zhao, Z. B.; Wan, W. B.; Gogotsi, Y.; Qiu, J. S. Ultralight and Highly Compressible Graphene Aerogels. *Adv. Mater.* **2013**, *25*, 2219–2223.
10. Xu, Z.; Liu, Z.; Sun, H. Y.; Gao, C. Highly Electrically Conductive Ag-Doped Graphene Fibers as Stretchable Conductors. *Adv. Mater.* **2013**, *25*, 3249–3253.
11. Jang, E. Y.; Carretero-González, J.; Choi, A.; Kim, W. J.; Kozlov, M. E.; Kim, T.; Kang, T. J.; Baek, S. J.; Kim, D. W.; Park, Y. W.; *et al.* Fibers of Reduced Graphene Oxide Nanoribbons. *Nanotechnology* **2012**, *23*, 235601–235609.
12. Li, X. M.; Zhao, T. S.; Wang, K. L.; Yang, Y.; Wei, J. Q.; Kang, F. Y.; Wu, D. H.; Zhu, H. W. Directly Drawing Self-Assembled, Porous, and Monolithic Graphene Fiber from Chemical Vapor Deposition Grown Graphene Film and Its Electrochemical Properties. *Langmuir* **2011**, *27*, 12164–12171.
13. Carretero-González, J.; Castillo-Martínez, E.; Dias-Lima, M.; Acik, M.; Rogers, D. M.; Sovich, J.; Haines, C. S.; Lepró, X.; Kozlov, M.; Zhakidov, A.; *et al.* Oriented Graphene Nanoribbon Yarn and Sheet from Aligned Multi-Walled Carbon Nanotube Sheets. *Adv. Mater.* **2012**, *24*, 5695–5701.
14. Zhao, Y.; Jiang, C. C.; Hu, C. G.; Dong, Z. L.; Xue, J. L.; Meng, Y. N.; Zheng, N.; Chen, P. W.; Qu, L. T. Large-Scale Spinning Assembly of Neat, Morphology-Defined, Graphene-Based Hollow Fibers. *ACS Nano* **2013**, *7*, 2406–2412.
15. Hu, C. G.; Zhao, Y.; Cheng, H. H.; Wang, Y. H.; Dong, Z. L.; Jiang, C. C.; Zhai, X. Q.; Jiang, L.; Qu, L. T. Graphene Microtubings: Controlled Fabrication and Site-Specific Functionalization. *Nano Lett.* **2012**, *12*, 5879–5884.
16. Xu, Z.; Zhang, Y.; Li, P. G.; Gao, C. Strong, Conductive, Lightweight, Neat Graphene Aerogel Fibers with Aligned Pores. *ACS Nano* **2012**, *6*, 7103–7113.
17. Jiang, K. L.; Li, Q. Q.; Fan, S. S. Nanotechnology: Spinning Continuous Carbon Nanotube Yarns. *Nature* **2002**, *419*, 801–801.
18. Liu, K.; Sun, Y. H.; Chen, L.; Feng, C.; Feng, X. F.; Jiang, K. L.; Zhao, Y. G.; Fan, S. S. Controlled Growth of Super-Aligned Carbon Nanotube Arrays for Spinning Continuous Unidirectional Sheets with Tunable Physical Properties. *Nano Lett.* **2008**, *8*, 700–705.
19. Zhang, M.; Atkinson, K. R.; Baughman, R. H. Multifunctional Carbon Nanotube Yarns by Downsizing an Ancient Technology. *Science* **2004**, *306*, 1358–1361.
20. Zhang, M.; Fang, S. L.; Zakhidov, A. A.; Lee, S. B.; Aliev, A. E.; Williams, C. D.; Atkinson, K. R.; Baughman, R. H. Strong, Transparent, Mmultifunctional, Carbon Nanotube Sheets. *Science* **2005**, *309*, 1215–1219.
21. Vigolo, B.; Pénicaud, A.; Coulon, C.; Sauder, C.; Pailler, R.; Journet, C.; Bernier, P.; Poulin, P. Macroscopic Fibers and Ribbons of Oriented Carbon Nanotubes. *Science* **2000**, *290*, 1331–1334.
22. Guo, F.; Kim, F.; Han, T. H.; Shenoy, V. B.; Huang, J. X.; Hurt, R. H. Hydration-Responsive Folding and Unfolding in Graphene Oxide Liquid Crystal Phases. *ACS Nano* **2011**, *5*, 8019–8025.
23. Yoo, E.; Okata, T.; Akita, T.; Kohyama, M.; Nakamura, J.; Honma, I. Enhanced Electrocatalytic Activity of Pt Subnanoclusters on Graphene Nanosheet Surface. *Nano Lett.* **2009**, *9*, 2255–2259.
24. Zhang, S.; Ji, C. Y.; Bian, Z. Q.; Yu, P. R.; Zhang, L. H.; Liu, D. Y.; Shi, E. Z.; Shang, Y. Y.; Peng, H. T.; Cheng, Q.; *et al.* Porous, Platinum Nanoparticle-Adsorbed Carbon Nanotube Yarns for Efficient Fiber Solar Cells. *ACS Nano* **2012**, *6*, 7191–7198.
25. Yang, Z. B.; Sun, H.; Chen, T.; Qiu, L. B.; Luo, Y. F.; Peng, H. S. Photovoltaic Wire Derived from Graphene Composite Fiber Achieving an 8.45% Energy Conversion Efficiency. *Angew. Chem., Int. Ed.* **2013**, *52*, 1–5.

26. Cheng, H. H.; Dong, Z. L.; Hu, C. G.; Zhao, Y.; Hu, Y.; Qu, L. T.; Chen, N.; Dai, L. M. Textile Electrodes Woven by Carbon Nanotube/Graphene Hybrid Fibers for Flexible Electrochemical Capacitors. *Nanoscale* **2013**, *5*, 3428–3434.
27. Cao, X. H.; Shi, Y. M.; Shi, W. H.; Lu, G.; Huang, X.; Yan, Q. Y.; Zhang, Q. C.; Zhang, H. Preparation of Novel 3D Graphene Networks for Supercapacitor Applications. *Small* **2011**, *7*, 3163–3168.